Stress orientations and magnitudes in the SAFOD pilot hole

Stephen Hickman[1] and Mark Zoback[2]

Received 19 March 2004; revised 13 July 2004; accepted 16 July 2004; published 13 August 2004.

[1] Borehole breakouts and drilling-induced tensile fractures in the 2.2-km-deep SAFOD pilot hole at Parkfield, CA, indicate significant local variations in the direction of the maximum horizontal compressive stress, S_{Hmax}, but show a generalized increase in the angle between S_{Hmax} and the San Andreas Fault with depth. This angle ranges from a minimum of 25 ± 10° at 1000–1150 m to a maximum of 69 ± 14° at 2050–2200 m. The simultaneous occurrence of tensile fractures and borehole breakouts indicates a transitional strike-slip to reverse faulting stress regime with high horizontal differential stress, although there is considerable uncertainty in our estimates of horizontal stress magnitudes. If stress observations near the bottom of the pilot hole are representative of stresses acting at greater depth, then they are consistent with regional stress field indicators and an anomalously weak San Andreas Fault in an otherwise strong crust. *INDEX TERMS:* 0915 Exploration Geophysics: Downhole methods; 5104 Physical Properties of Rocks: Fracture and flow; 7209 Seismology: Earthquake dynamics and mechanics; 8010 Structural Geology: Fractures and faults; 8164 Tectonophysics: Stresses—crust and lithosphere. **Citation:** Hickman, S., and M. Zoback (2004), Stress orientations and magnitudes in the SAFOD pilot hole, *Geophys. Res. Lett.*, *31*, L15S12, doi:10.1029/2004GL020043.

1. Introduction

[2] Many of the issues to be addressed by drilling into the San Andreas Fault (SAF) have evolved from the long-standing debate regarding the magnitude of shear stress resisting slip over the upper 15–20 km of the fault. This long-term average shear stress is a measure of fault strength. A "weak" SAF is one whose strength is <20 MPa while a "strong" SAF would have a strength ~50–100 MPa, as expected on the basis of laboratory-derived coefficients of friction (μ) of 0.6–1.0 [*Byerlee*, 1978] assuming hydrostatic pore pressures ("Byerlee's law"). Stress measurements in a variety of tectonic settings indicate that strengths of active faults within plate interiors are comparable to those predicted by Byerlee's Law [see *Townend and Zoback*, 2000].

[3] Despite the evidence for strong intraplate faults, the absence of frictionally generated heat in shallow boreholes first suggested that the SAF is weak [e.g., *Brune et al.*, 1969; *Lachenbruch and Sass*, 1980]. Analyses of earthquake focal mechanisms, borehole breakouts and hydraulic fractures indicate that the direction of the maximum horizontal principal stress, S_{Hmax}, is generally at high angles (about 65–85°) to the SAF, suggesting that the fault is sliding at very low levels of shear stress [e.g., *Zoback et al.*, 1987; *Mount and Suppe*, 1987; *Townend and Zoback*, 2004]. Furthermore, measurements of stress and heat flow to depths of 3.5 km in the Cajon Pass hole in southern California indicate high differential stresses adjacent to the SAF (i.e., a strong crust) but suggest that the SAF itself is relatively weak [*Zoback and Healy*, 1992; *Lachenbruch and Sass*, 1992]. Measurements of heat flow in the 2.2-km-deep pilot hole drilled for the San Andreas Fault Observatory at Depth (SAFOD) confirm these earlier studies, and show no evidence for frictionally generated heat adjacent to the SAF in central California [*Williams et al.*, 2004]. Taken together, these observations suggest that the SAF is a weak fault in an otherwise strong crust.

[4] In spite of strong observational support for S_{Hmax} being at high angles to the SAF, in some locations the azimuth of S_{Hmax} rotates to make a more acute angle with the SAF as the fault is approached [*Hardebeck and Hauksson*, 2001]. This rotation was used by *Scholz* [2000] to argue that the SAF was strong, although the magnitude of this rotation has been debated because of the paucity of data close to the SAF and inherent difficulties in inverting focal mechanisms for stress directions when the number and diversity of focal mechanisms is small [*Hardebeck and Hauksson*, 2001; *Townend and Zoback*, 2004]. The primary goal of the present study is thus to obtain independent constraints on the orientations and magnitudes of the horizontal principal stresses from observations of borehole failure in the SAFOD pilot hole, located only 1.8 km from the surface trace of the SAF near the town of Parkfield, California.

2. Stress Orientations

[5] After passing through 760 m of Tertiary and Quaternary sedimentary rocks, the SAFOD pilot hole was drilled through Salinian granite basement to a depth of 2.17 km and then logged with an extensive suite of wireline geophysical tools [see *Boness and Zoback*, 2004]. This included both the Ultrasonic Borehole Imager (UBI) and Formation Microimager (FMI) tools. These tools produce oriented images of borehole wall reflectivity, radius and microresistivity, from which the geometry and orientation of fractures, faults, borehole irregularities, and lithologic units can be determined. High-quality UBI and FMI logs were obtained over the entire open-hole interval of the pilot hole. These logs were crosschecked against each other and against independent borehole directional surveys to verify that the images obtained were accurately oriented.

[6] The UBI and FMI logs revealed extensive stress-induced borehole breakouts and, to a lesser extent, drilling-induced tensile wall fractures throughout much of the pilot hole (Figure 1a). Borehole breakouts and drilling-induced tensile cracks form through compressive and tensional rock failure in response to tectonic stress concentrations at the

[1]U. S. Geological Survey, Menlo Park, California, USA.
[2]Department of Geophysics, Stanford University, Stanford, California, USA.

0094-8276/04/2004GL020043$05.00

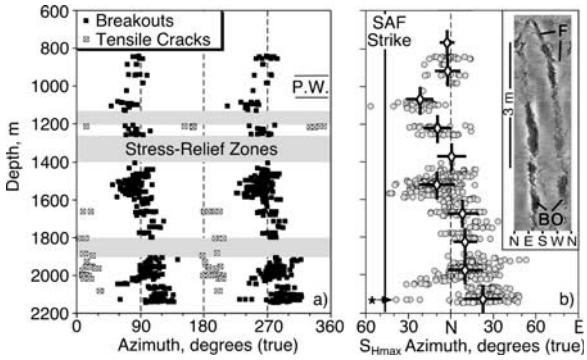

Figure 1. Azimuths of a) stress-induced borehole breakouts and tensile cracks and b) maximum horizontal compressive stress, S_{Hmax}, vs. depth in the SAFOD pilot hole. The mean orientations of S_{Hmax} over ten discrete 150 m depth intervals are shown as open diamonds. The vertical bars represent the depth range of each interval and the horizontal bars the angular standard deviation. The local strike of the San Andreas Fault (SAF; N 46°W) is shown for reference. Inset) Ultrasonic Borehole Imager (UBI) log showing a dramatic rotation in breakout (BO) azimuth in proximity to a fault (F) at 2126 m (* in Figure 1b). Extensive pipe wear (P.W.) degraded the quality of the UBI log at 945–1060 m, thus the true breakout density over this depth interval may exceed that shown here.

borehole wall, but along azimuths that differ by 90° (Figure 1a). Numerous field studies have shown that breakouts and tensile cracks yield reliable information on the orientation of the horizontal principal stresses [see *Zoback et al.*, 2003]. The deviation of the pilot hole from vertical was <3° over most of its length, and never exceeded 6°. Thus, the potential effects of borehole deviation on breakout and tensile crack azimuths can be safely neglected in this study.

[7] The azimuths of S_{Hmax} indicated by breakouts and tensile cracks in the pilot hole exhibit significant local variability over depths ranging from a few meters to several hundred meters (Figure 1b). A particularly dramatic example of a localized stress rotation, wherein the apparent azimuth of S_{Hmax} changes by about 70° over a depth of only 5 m, was seen just below a minor fault at 2126 m (Figure 1b, inset). Similar localized stress rotations have been observed near faults in other boreholes, especially in tectonically active areas, and have been successfully modeled as resulting from slip on these faults [e.g., *Barton and Zoback*, 1994]. Thus, we hypothesize that many of the localized stress rotations seen in the pilot hole probably result from slip on nearby faults and are indicative of active deformation in the crust adjacent to the SAF. These slip events could occur at a variety of scales, ranging from relatively small faults seen in the pilot hole image logs [*Boness and Zoback*, 2004] to larger faults imaged using the pilot hole seismic array [*Chavarria et al.*, 2003].

[8] To quantify variations in S_{Hmax} azimuth with depth, we grouped the data into discrete 150 m depth intervals starting at 700 m and used Fisher statistics to compute the angular mean and standard deviation over these intervals (Figure 1b). This analysis shows that the angle between S_{Hmax} and the local strike of the SAF is relatively acute in the upper part of the hole and changes with depth from 44 ± 9° at 850–1000 m to 25 ± 10° at 1000–1150 m and then to 37 ± 13° at 1450–1600 m. Below 1600 m, however, the angle between S_{Hmax} and the strike of the SAF steadily increases to 55 ± 11° at 1600–1750 m and then to 69 ± 14° at 2050–2200 m. Although the angle between S_{Hmax} and the SAF averaged over the entire pilot hole is rotated with respect to other regional stress indicators, the angle between S_{Hmax} and the SAF at depths of 2050–2200 m is similar to that observed in central California at greater distances from the SAF (Figure 2) [*Townend and Zoback*, 2004]. S_{Hmax} orientations at the bottom of the pilot hole also agree with inversions of focal mechanisms from microearthquakes along the creeping section of the SAF (starting about 10 km northwest of the pilot hole), which indicate that S_{Hmax} is generally at angles of 65–85° to the SAF, both in the far field and even at distances as small as 1–3 km from the fault [*Provost and Houston*, 2001].

3. Stress Magnitudes

[9] Although we intended to collect core samples and conduct a hydraulic fracturing stress measurement at the bottom of the pilot hole, a logging tool stuck in the bottom of the hole forced us to delay these activities until drilling of the main SAFOD hole. Instead, as discussed by *Moos and Zoback* [1990] and *Zoback et al.* [2003], we were able to use the observation that breakouts and drilling-induced tensile fractures occurred together over certain depth intervals in the pilot hole (Figure 1a) to estimate the magnitudes of S_{Hmax} and the least horizontal principal stress, S_{hmin}. These estimates were derived from theoretical models for the elastic concentration of stresses around a circular borehole, using data on unconfined compressive strength (C_o), tensile strength (T), formation fluid pressure, drilling mud weight, extent of wellbore cooling, breakout width and

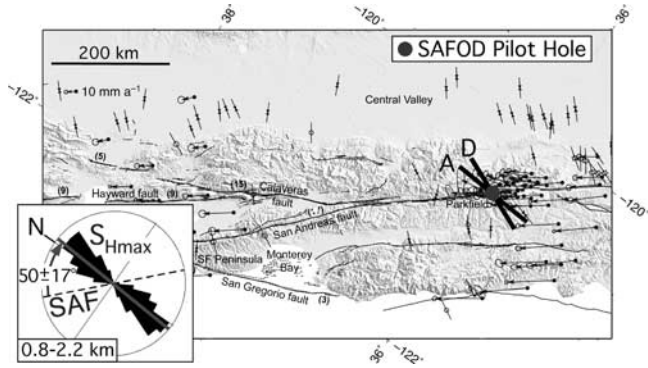

Figure 2. Azimuth of S_{Hmax} from the pilot hole compared to other stress direction indicators in central California. S_{Hmax} directions from borehole breakouts, hydraulic fracturing tests, and earthquake focal mechanisms are shown as inward-pointing arrows, stars and split circles, respectively [*Townend and Zoback*, 2004]. The mean azimuth of S_{Hmax} from the pilot hole is shown as solid black lines, both for all depths (A) and for only the deepest part of the hole (D; 2050–2200 m). Vectors show plate motions from *Murray and Segall* [2001]. Inset) Rose diagram of S_{Hmax} directions from all depths in the pilot hole relative to the local strike of the San Andreas Fault (SAF). The mean azimuth of S_{Hmax} is shown as a grey line.

elastic properties. For the pilot hole, most of these parameters (e.g., magnitude of borehole cooling, drilling mud weight, breakout width) were determined directly from drilling records or wireline geophysical logs; other parameters were either estimated (formation fluid pressure) or obtained from laboratory tests on granites from other localities (elastic properties, rock strength).

[10] To carry out these stress estimates, C_o was obtained from direct measurements of the in-situ P-wave velocity (V_P) [see *Boness and Zoback*, 2004] and an empirical correlation between V_P and C_o in core samples of Lac du Bonnet granite from depths up to 1 km [*Annor and Jackson*, 1987]:

$$C_o = 129 + 14.5V_P \quad (1)$$

where C_o is in MPa and V_P is in km/s. The values of C_o derived from equation (1) ranged from 197–212 MPa (Figure 3a), with uncertainties (illustrated in Figure 3 for a depth of 1671 m) obtained from a statistical analysis of the *Annor and Jackson* [1987] data. Similar values for C_o (about 10 MPa higher) were obtained from the pilot hole well logs using an empirical correlation between C_o and dynamic Young's modulus for crystalline igneous and metamorphic rocks [*Strohmeyer*, 2003]. We also made the reasonable assumption [*Jaeger and Cook*, 1976] that T for pilot hole granites ranged from about 10% of the peak C_o (i.e., 20 MPa) to 0 MPa, the latter value allowing for rock that was already fractured at the borehole wall. Although the values we used for C_o are in accord with the range of values measured on granites in the laboratory [*Lockner*, 1995], they are only a proxy for actual measurements of C_o that will be made on core samples from the main SAFOD hole. Thus, the stress magnitudes presented in this paper are only

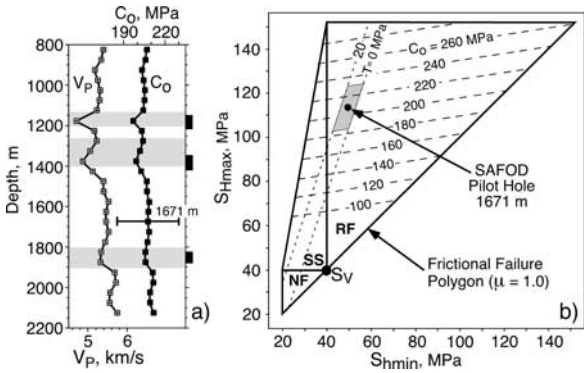

Figure 3. a) P-wave velocity (50 m averages) and estimates of unconfined compressive strength (C_o) for granites penetrated by the pilot hole. Also shown are stress relief zones (grey bands) from Figure 1a and shear zones identified by *Boness and Zoback* [2004] (black rectangles). b) Stress constraint from depth of 1671 m. Contours of C_o and tensile strength (T) are shown as long and short dashed lines, respectively. Limits on S_{Hmax} and S_{hmin} imposed by the frictional strength of the crust are shown as solid black lines, with NF, SS and RF denoting normal, strike-slip and reverse faulting stress regimes. Black dot and surrounding grey rhomboid indicate values of C_o and T used, with uncertainties (see Figure 3a).

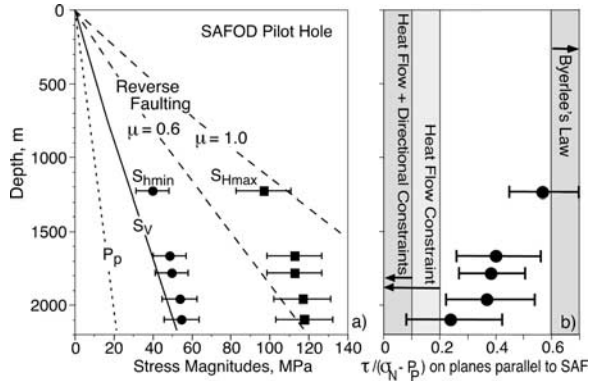

Figure 4. a) Estimated stress magnitudes in the pilot hole. Dashed lines indicate S_{Hmax} at which frictional failure would occur along optimally oriented reverse faults for hydrostatic fluid pressures and $\mu = 0.6–1$ (Byerlee's Law). b) Ratio of shear stress (τ) to effective normal stress ($\sigma_N - P_p$) resolved onto planes parallel to the San Andreas Fault. Also shown are upper bounds to $\tau/(\sigma_N - P_p)$ allowed along the San Andreas Fault by the heat flow and stress direction constraints and the lower bound allowed by Byerlee's Law. Error bars reflect the combined effects of uncertainties in stress orientations, rock strengths and other parameters.

estimates, pending comprehensive hydraulic fracturing stress measurements and laboratory strength testing planned for SAFOD.

[11] An example of a stress constraint analysis for the pilot hole following the methodology of *Moos and Zoback* [1990] and using our estimates of C_o and T is shown in Figure 3b. This analysis indicates that the magnitudes of S_{hmin} and S_{Hmax} at a depth of about 1671 m are 49 ± 9 MPa and 113 ± 14 MPa, respectively. Stress estimates were obtained in this manner for five different depth intervals in the pilot hole (Figure 4a). The magnitude of the vertical stress (S_v) was calculated from the pilot hole density log [*Boness and Zoback*, 2004] and the pore pressure (P_p) was calculated assuming hydrostatic equilibrium with a surface water table for a fluid density of 1 gm/cm^3. This analysis shows that the magnitude of S_{hmin} in the pilot hole is approximately equal to S_v, indicative of a transitional strike-slip to reverse faulting stress regime. Also, the magnitude of S_{Hmax} is significantly greater than S_v and at the critical value for incipient reverse faulting as predicted by Byerlee's Law (Figure 4a). Overall, these results are consistent with the style of active deformation in the central Coast Ranges as well as focal mechanisms from microearthquakes off the main trace of the San Andreas Fault in the Parkfield area [*Eberhart-Phillips and Michael*, 1993].

4. Stress Relief Zones

[12] Three depth intervals in the pilot hole were notably free of borehole breakouts: 1130–1205 m, 1260–1400 m, and 1800–1905 m (Figure 1a). Since breakout formation is inhibited either by an increase in C_o or a decrease in horizontal differential stress ($S_{Hmax} - S_{hmin}$), and given that C_o in these three intervals is either equal to or slightly lower than that observed elsewhere in the hole (Figure 3a), we interpret these breakout-free zones to be due to local

stress relief associated with slip on faults penetrated by the pilot hole. In fact, these stress relief zones are located close to three major shear zones identified in the pilot hole by *Boness and Zoback* [2004] on the basis of anomalously low seismic velocities and rock density as well as high velocity anisotropy (see black boxes in Figure 3a).

5. Implications for San Andreas Fault Strength

[13] *Chéry et al.* [2004] modeled the SAF as a vertical fault cutting a 25-km-deep crust and underlying mantle, assuming an elastic-frictional rheology at low temperature and a viscoelastic rheology at high temperature. They found that the S_{Hmax} orientation near the bottom of the pilot hole, the overall clockwise rotation in S_{Hmax} with depth, and the high horizontal differential stresses ($S_{Hmax} - S_{hmin}$) were all compatible with a weak SAF ($\mu < 0.1$) embedded in a strong crust and weak upper mantle. However, they predicted less overall rotation in S_{Hmax} than observed in the pilot hole and did not reproduce the localized perturbations in S_{Hmax} azimuth seen, which suggest that other, local factors may also influence the stress field at this site. Nevertheless, their model, in conjunction with the pilot hole stress constraints and in the context of regional stress orientations [*Townend and Zoback*, 2004; *Provost and Houston*, 2001], suggests that strong SAF/strong crust models like that of *Scholz* [2000] are not applicable to the SAF near Parkfield.

[14] We conclude by considering the more general implications of our data for fault strength. From the measured S_{Hmax} orientations (Figure 1b) and estimates of S_{Hmax} and S_{hmin} magnitudes and P_p (Figure 4a), the ratio of shear to effective normal stress on planes parallel to the SAF can be computed, which represents the apparent coefficient of friction required for right-lateral strike-slip failure along San-Andreas-parallel faults. This ratio is consistent with Byerlee's Law at shallow depths but approaches low values (0.24) at the bottom of the pilot hole (Figure 4b). Thus, if the stress state at the bottom of the pilot hole is representative of stresses acting on the actively deforming SAF at greater depth, then we tentatively conclude that our observations are consistent with regional stress direction indicators and a weak SAF/strong crust model. However, the full significance of our pilot hole stress measurements for the strength of the SAF will not be known until we make direct, in-situ stress measurements at greater depth and across the San Andreas Fault Zone with SAFOD.

[15] **Acknowledgments.** We gratefully acknowledge the International Continental Scientific Drilling Program for funding drilling and testing of the SAFOD pilot hole and the U.S. Geological Survey Earthquake Hazards Program and National Science Foundation (grant NSF-EAR-0208493) for funding the activities of Hickman and Zoback, respectively. We thank Art McGarr, Jeanne Hardebeck and three anonymous reviewers for their very constructive comments on this paper.

References

Annor, A., and R. Jackson (1987), Mechanical, thermal and joint properties of rock samples from the Lac du Bonnet Batholith, Manitoba, in *Geotechnical Studies at Whiteshell Research Area (RA-3)*, edited by T. J. Katsube and J. P. Jume, *Div. Rep. MRL 87-52*, CANMET Min. Res. Lab., Ottawa.

Barton, C. A., and M. D. Zoback (1994), Stress perturbations associated with active faults penetrated by boreholes: Possible evidence for near-complete stress drop and a new technique for stress magnitude measurements, *J. Geophys. Res.*, *99*, 9373–9390.

Boness, N., and M. D. Zoback (2004), Stress-induced seismic velocity anisotropy and physical properties in the SAFOD pilot hole in Parkfield, CA, *Geophys. Res. Lett.*, *31*, L15S17, doi:10.1029/2003GL019020.

Brune, J. N., T. L. Henyey, and R. F. Roy (1969), Heat flow, stress, and rate of slip along the San Andreas fault, California, *J. Geophys. Res.*, *74*, 3821–3827.

Byerlee, J. D. (1978), Friction of rocks, *Pure Appl. Geophys.*, *116*, 615–626.

Chavarria, J. A., P. E. Malin, R. D. Catchings, and E. Shalev (2003), A look inside the San Andreas fault at Parkfield through vertical seismic profiling, *Science*, *302*, 1746–1748.

Chéry, J., M. D. Zoback, and S. Hickman (2004), A mechanical model of the San Andreas fault and SAFOD pilot hole stress measurements, *Geophys. Res. Lett.*, *31*, L15S13, doi:10.1029/2004GL019521.

Eberhart-Phillips, D., and A. J. Michael (1993), Three-dimensional velocity structure, seismicity, and fault structure in the Parkfield region, central California, *J. Geophys. Res.*, *98*, 15,737–15,758.

Hardebeck, J. L., and E. Hauksson (2001), Crustal stress field in southern California and its implications for fault mechanics, *J. Geophys. Res.*, *106*, 21,859–21,882.

Jaeger, J. C., and N. G. W. Cook (1976), *Fundamentals of Rock Mechanics*, 2nd ed., 585 pp., Chapman and Hall, New York.

Lachenbruch, A. H., and J. H. Sass (1980), Heat flow and energetics of the San Andreas fault zone, *J. Geophys. Res.*, *85*, 6185–6223.

Lachenbruch, A. H., and J. H. Sass (1992), Heat flow from Cajon Pass, fault strength, and tectonic implications, *J. Geophys. Res.*, *97*, 4995–5015.

Lockner, D. A. (1995), Rock failure, in *Rock Physics and Phase Relations: A Handbook of Physical Constants*, edited by T. Ahrens, pp. 127–147, AGU, Washington, D. C.

Moos, D., and M. D. Zoback (1990), Utilization of observations of well bore failure to constrain the orientation and magnitude of crustal stresses: Application to continental, Deep Sea Drilling Project, and Ocean Drilling Program boreholes, *J. Geophys. Res.*, *95*, 9305–9325.

Mount, V. S., and J. Suppe (1987), State of stress near the San Andreas fault: Implications for wrench tectonics, *Geology*, *15*, 1143–1146.

Murray, M. H., and P. Segall (2001), Modeling broadscale deformation in northern California and Nevada from plate motions and elastic strain accumulation, *Geophys. Res. Lett.*, *28*, 4315–4318.

Provost, A.-S., and H. Houston (2001), Orientation of the stress field surrounding the creeping section of the San Andreas fault: Evidence for a narrow mechanically weak fault zone, *J. Geophys. Res.*, *106*, 11,373–11,386.

Scholz, C. H. (2000), Evidence for a strong San Andreas fault, *Geology*, *28*, 163–166.

Strohmeyer, D. (2003), Gefügeabhängigkeit technischer Gesteinseigenschaften, Ph.D. dissertation, 319 pp., Univ. Göttingen, Göttingen, Germany.

Townend, J., and M. D. Zoback (2000), How faulting keeps the crust strong, *Geology*, *28*, 399–402.

Townend, J., and M. D. Zoback (2004), Regional tectonic stress near the San Andreas fault in central and southern California, *Geophys. Res. Lett.*, *31*, L15S11, doi:10.1029/2003GL018918.

Williams, C. F., F. V. Grubb, and S. P. Galanis (2004), Heat flow in the San Andreas Fault Observatory (SAFOD) pilot hole and implications for the strength of the San Andreas fault, *Geophys. Res. Lett.*, *31*, L15S14, doi:10.1029/2003GL019352.

Zoback, M. D., and J. H. Healy (1992), In situ stress measurements to 3.5 km depth in the Cajon Pass scientific research borehole: Implications for the mechanics of crustal faulting, *J. Geophys. Res.*, *97*, 5039–5057.

Zoback, M. D., et al. (1987), New evidence for the state of stress on the San Andreas fault system, *Science*, *238*, 1105–1111.

Zoback, M. D., C. Barton, M. Brudy, D. Castillo, T. Finkbeiner, B. Grollimund, D. Moos, P. Peska, C. Ward, and D. Wiprut (2003), Determination of stress orientation and magnitude in deep wells, *Int. J. Rock Mech. Min. Sci. Geomech. Abstr.*, *40*, 1049–1076.

S. Hickman, U. S. Geological Survey, 345 Middlefield Road, Menlo Park, CA 94025, USA. (hickman@usgs.gov)

M. Zoback, Department of Geophysics, Stanford University, Stanford, CA, USA.